

Femtosecond photoexcitation dynamics inside a quantum solvent

Bernhard Thaler¹, Sascha Ranftl¹, Pascal Heim¹, Stefan Cesnik¹, Leonhard Treiber¹, Ralf Meyer¹, Andreas W. Hauser¹, Wolfgang E. Ernst¹, and Markus Koch^{*1}

¹Graz University of Technology, Institute of Experimental Physics, Petersgasse 16, 8010 Graz, Austria

Abstract

The observation of chemical reactions on the time scale of the motion of electrons and nuclei has been made possible by lasers with ever shortened pulse lengths. Superfluid helium represents a special solvent that permits the synthesis of novel classes of molecules that have eluded dynamical studies so far. However, photoexcitation inside this quantum solvent triggers a pronounced response of the solvation shell, which is not well understood. Here we present a mechanistic description of the solvent response to photoexcitation of indium (In) dopant atoms inside helium nanodroplets (He_N), obtained from femtosecond pump-probe spectroscopy and time-dependent density functional theory simulations. For the In- He_N system, part of the excited state electronic energy leads to expansion of the solvation shell within 600 fs, initiating a collective shell oscillation with a period of about 30 ps. These coupled electronic and nuclear dynamics will be superimposed on intrinsic photoinduced processes of molecular systems inside helium droplets.

Introduction

Since the award of the 1999 Nobel Prize for Chemistry [1], various fundamental molecular processes have been investigated on their natural time scales, e.g. fragmentation via different pathways on the molecular potential energy surface [2], non-adiabatic electron-nuclear coupling [3], or electron dynamics initiated by ultrashort laser pulses [4]. Superfluid helium nanodroplets (He_N) have been used as nanocryostats to isolate atoms or molecules at 0.4 K temperature, or to form new weakly bound aggregates [5, 6]. Their gentle influence on guest particles is demonstrated, for example, by electron spin resonance [7] or molecular rotation and alignment experiments [8, 9]. He droplets are an appealing spectroscopic tool because of their transparency for electromagnetic radiation up to the extreme ultraviolet energy regime [5]. However, photoexcitation inside the droplet leads to dissipation of significant excess energy via coupling to collective modes of the surrounding helium, which is expected to be a fast process. Femtochemistry inside He_N will allow real time tracking of photochemical reactions in novel systems, such as fragile agglomerates [10, 11, 12], or molecules in a microsolvation environment [13]. This will, however, require a detailed knowledge about the response of the quantum fluid to the photoexcitation of a dopant atom or molecule. So far, only the ultrafast dynamics in pure helium droplets have been studied [14], and femtosecond measurements on doped helium droplets were restricted to the surface bound alkali metals [15, 16] that can hardly couple to helium bubble modes. Since most foreign atoms and molecules reside inside the droplets and couple more strongly, we have concentrated on the electronic excitation of single atoms well inside the droplets. In this way, no other degrees of freedom such as rotation or vibration would interact and only the coupling of the electronic excitation with the modes of the surrounding helium should be detected. Previous spectroscopic studies in the frequency domain have shown blue-shifted excitation bands of dopants inside droplets compared to gas phase indicating that an excess energy is required to create a correspondingly larger helium bubble to accommodate the excited electron orbital [5]. This excess energy must be released to the helium in form of a damped helium excitation mode.

In our work, we follow the expansion of the helium bubble after electronic excitation of single indium (In) dopants in real time. After an expansion from 4.5 Å to 8.1 Å radius in 600 fs, we observe a contraction of the surrounding He at (28 ± 1) ps, as well as an ejection of the dopant atom from the droplet about 60 ps after the electronic excitation. As observable in our fs pump-probe measurements, we chose the photoelectrons released because they have been shown to exit the droplet rather ballistically without being significantly influenced by the helium environment [15, 14, 17]. In spite of its importance for photochemical studies in superfluid helium droplets, this sequence of events has not previously been observed.

Results

Photoexcitation dynamics of the In- He_N system. We investigate photoexcitation dynamics of the In- He_N system with a combination of time-resolved photoelectron spectroscopy (TRPES) and time-dependent density functional theory (TDDFT) simulation, as described in the following. A mechanistic description of the processes deduced from experiment and theory will be discussed in the final paragraph.

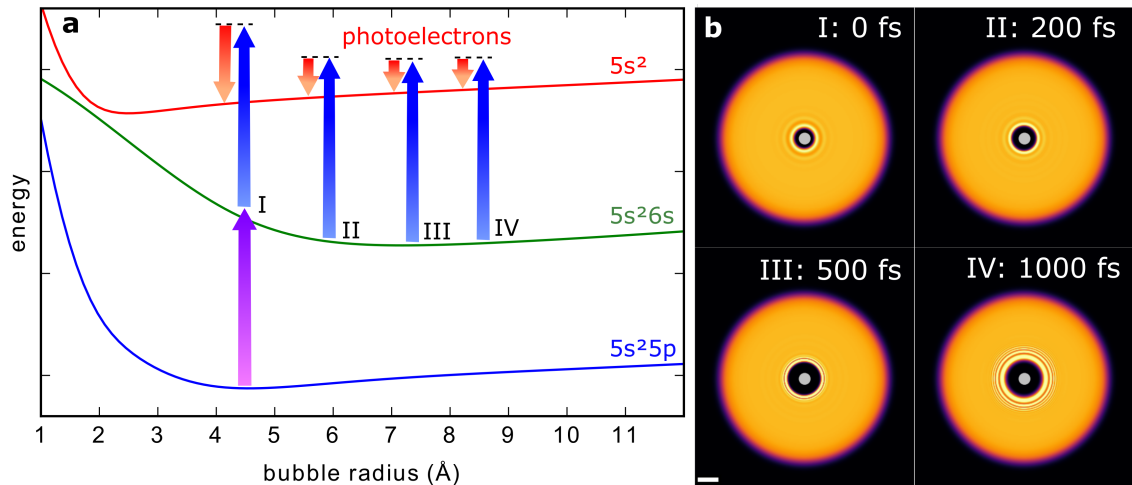


Figure 1: Temporal evolution of the In-He_N system after photoexcitation. (a) Sketch of the In-He_N potential energy surfaces as function of the bubble radius for In in its ground [$5s^2 5p$ ($^2P_{1/2}$), blue], lowest excited [$5s^2 6s$ ($^2S_{1/2}$), green] and ionic ground state [$5s^2$ (1S_0), red]. The purple arrow indicates pump excitation at 376 nm, blue arrows indicate probe ionization at 405 nm for characteristic delay times and red arrows correspond to the PE kinetic energy, as measured by TRPES. (b) Helium density distributions of a He₄₀₀₀ droplet with an In atom located in the centre for selected times after photoexcitation, as calculated with TDDFT. Scale bars, 10 Å.

Time-resolved photoelectron spectroscopy

The feasibility of ultrafast experiments inside He_N ultimately depends on the availability of an experimental observable that is available with sufficiently low distortion by the intermediate helium. Ion detection, as used on the droplet surface, is not possible because ions are captured inside the droplet due to their attractive potential [15]. Photoelectron (PE) detection, in contrast, has been successfully used for pure and doped He_N [17, 15, 14]. TRPES is a well established method for ultrafast gas-phase studies and is primarily sensitive to the electronic structure of a system [18, 19]. As depicted in figure 1a, after photoexcitation by a pump pulse the evolution of the excited state is probed by time-delayed photoionization and the PE kinetic energy (red arrows) is measured. When applied inside a He_N, photoexcitation induces an abrupt disturbance of the quantum fluid solvation shell due to expansion of the valence electron wave function. Because the energies of the electronic states depend on the structure of the He environment, the transient response of the quantum solvent can be sensed with TRPES (see figure 1a).

Figure 2 shows the time-dependent evolution of the PE signal within the first picosecond after photoexcitation (a), together with PE spectra at selected pump-probe times (b). Within about 600 fs the PE peak energy is shifted from 0.61 eV to 0.34 eV, followed by a slower decrease to 0.32 eV at 1000 fs, which is about 0.02 eV above the gas-phase peak that appears at around 0.30 eV (solid line in figure 2). The remaining shift represents the reduced ionization potential of In atoms in the He environment due to polarization effects [17]. The linewidth of the PE spectra is significantly increased and changes within the first picosecond (figure 2b), which we ascribe to the following four reasons: First, during pump-probe cross correlation of 150 fs, saturation effects and the spectral width of the pump pulse are expected to contribute to the PE linewidth. Second,

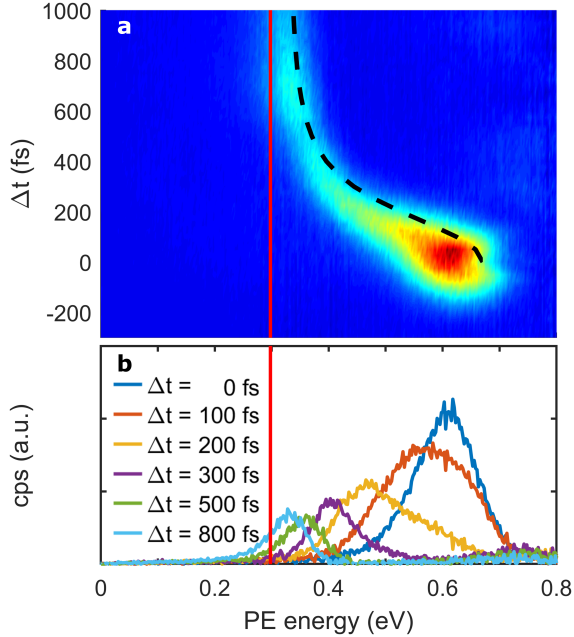


Figure 2: Time-resolved photoelectron (PE) spectra of single In atoms solvated inside He_N . The average droplet size is 4000 He atoms. (a) PE kinetic energy spectrum as function of the pump-probe time delay Δt , together with the simulated dynamics (dashed line) and the gas-phase PE energy (solid line). Around time-zero the PE signal is increased due to temporal overlap of the pump and probe pulses. Additionally, the total PE signal decreases during the expansion, which might be due to a decreased ionization probability for larger bubbles and/or lower escape probability of slow electrons from larger bubbles at long delays compared to fast electrons from small bubbles at short delays [20, 17]. (b) Selected spectra for different pump-probe time delays, which resemble horizontal cuts through the 2D plot in (a).

within the first 500 fs, a peak shift with a maximum slope of about 1 meV/fs in combination with the 150 fs pump-probe cross correlation leads to an expected contribution of about 150 meV. Third, ionization inside the droplet increases the linewidth, given by the Franck-Condon overlap of the excited and the ionic state (c.f., figure 1), which seems to be the dominant contribution to the linewidth after 500 fs. Fourth, relaxation of the photoelectrons due to binary collisions with individual He atoms on the way out of the droplet leads to an asymmetric shape of the PE peaks [17]. These decelerated electrons can be seen as wing extending to PE energies below the gas phase value (red line in figure 2b and Supplementary Fig. 7b).

In figure 3 the PE kinetic energy up to 100 ps is shown (blue dots). After a steep decrease representing the tail of the initial peak shift shown in figure 2, the peak position slowly decreases to reach a constant value at about 60 ps with a temporary increase at (28 ± 1) ps. The PE peak width shows a very similar trend (figure 3, red diamonds) with a steady decrease over time to about 35 meV at long time delays and a temporary increase. Detailed scans of PE peaks at short and long time delays are shown in Supplementary Fig. 7b. We note that except for very short time delays right after the pump-probe overlap (cross-correlation), the total PE yield stays constant over the whole investigated temporal region.

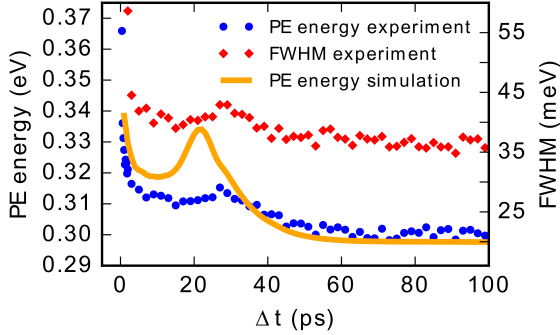


Figure 3: Photoelectron (PE) peak position and linewidth as function of time delay Δt . The transient peak position (blue dots) and full width at half maximum (FWHM, red diamonds) are shown within 100 ps after photoexcitation, as measured with TRPES and simulated with TDDFT (orange line). The experimental peak position and FWHM are obtained by Gaussian fits to the corresponding PE energy spectra. The start position for the TDDFT simulation was 20 Å from the droplet center in order to obtain a similar ejection behavior as the experiment.

Time-dependent helium density functional theory

To obtain further insight into the ultrafast dynamics, photoexcitation of the In-He_N system is simulated with TDDFT using the BCN-TLS-He-DFT computing package [21], which has been successfully applied to reproduce the dynamics of He_N loaded with various different atomic species [22]. In the present case, an extraordinary amount of excess energy of several hundred meV is coupled into the system in the photoexcitation process. We therefore carefully tested the simulations for convergence by variation of the simulation parameters (see Supplementary Note 3 and Supplementary Figs. 4 and 5).

figure 1b shows He density distributions for selected times after photoexcitation and the corresponding bubble expansion over time is plotted in figure 4a. Inside the droplet the energies of the In excited state ($5s^26s$) and its ionic state ($5s^2$) deviate from the bare atom values by the interaction energies $E_{\text{He}_N\text{-In}^*}$ and $E_{\text{He}_N\text{-In}^+}$, respectively. These interaction energies, plotted in figure 4b, are calculated by integrating the respective In-He pair potentials over the He density. While $E_{\text{He}_N\text{-In}^*}$ (cyan curve) is positive and decreases with time (for larger bubbles), $E_{\text{He}_N\text{-In}^+}$ (red curve) is negative and increases. This behavior can be expected from the repulsive and attractive character of the excited and ionic state pair potentials, respectively (Supplementary Fig. 3). The simulated PE peak shift with respect to the free atom, as plotted in figure 4c, is calculated as the difference of the two interaction energies ($E_{\text{He}_N\text{-In}^*} - E_{\text{He}_N\text{-In}^+}$) and compared to the measured transient peak shift in figures 2a and 4c, revealing good agreement. Note that within 1000 fs $E_{\text{He}_N\text{-In}^*}$ decreases to zero, whereas $E_{\text{He}_N\text{-In}^+}$ is negative and reaches zero only at higher time delays. This results in a further peak shift between 1000 fs and 60 ps (see figure 3), as the dopant is ejected from the droplet. As can be seen in figure 4c, below 200 fs the experimental peak shifts are slightly lower than the simulated ones, which we ascribe to a distortion of the PE peaks due to a cross correlation signal caused by overlap of pump and probe pulses in this temporal region (c.f., figure 2b).

Next, we compare the steady decrease of the excited state electronic energy (cyan curve in figure 4b) to the kinetic energy of the helium atoms (dashed line in figure 4b), and find that the two curves show almost exactly complementary trends.

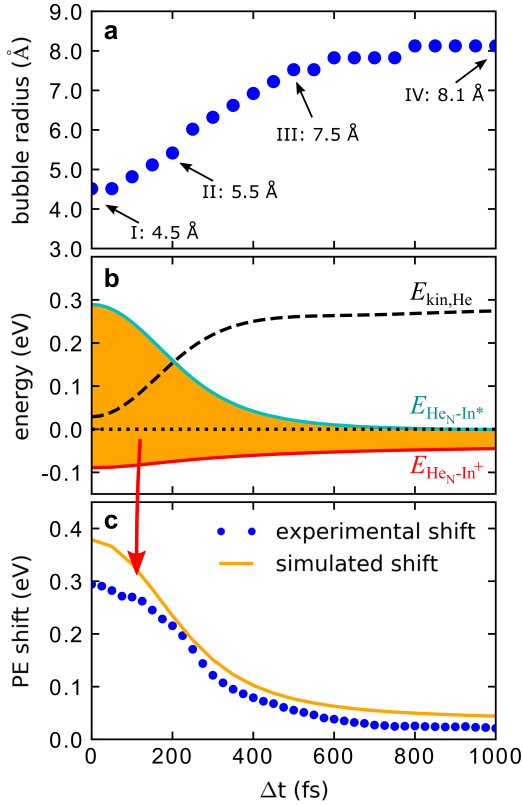


Figure 4: Photoexcitation (PE) dynamics of the In-He₄₀₀₀ system simulated with TDDFT. (a) Bubble radius as a function of time delay Δt , determined as position of the corresponding He distribution at which the density has dropped to 50% of the bulk value. Times for which the calculated He density is shown in figure 1b are indicated. (b) Interaction energy $E_{\text{He}_N\text{-In}^*}$ of the $5s^26s$ excited state (cyan curve) and interaction energy $E_{\text{He}_N\text{-In}^+}$ of the $5s^2$ ionic state (red curve). Additionally, the kinetic energy of the He atoms, $E_{\text{kin, He}}$, is plotted as dashed line. (c) Simulated PE peak shift induced by the He environment (orange line), obtained as $E_{\text{He}_N\text{-In}^*} - E_{\text{He}_N\text{-In}^+}$ (indicated by the shaded area in (b)), which is also shown in figure 2a. For comparison to the measured shift of the PE peak position over time, the recorded electron spectra at all time delays (c.f., figure 2b) are fitted with Gaussian functions and the line positions are indicated here by blue dots.

Finally, the simulated PE peak position for an In atom, that is photoexcited at a distance of 20 Å from the droplet center, is shown in figure 3 (orange line). The choice of this position is justified by comparing simulated PE peak transients with different starting positions (see Supplementary Note 4 and Supplementary Fig. 6). The simulated curve shows the same overall decrease as the experimental values (blue dots), although with a more pronounced temporal increase at 22 ps.

Discussion

The transient shift in the pump-probe PE spectrum of the In-He_N system within the first ps (figure 2) has to be related to solvation shell dynamics, as no internal degrees of freedom are available for relaxation of the In atom in its lowest electronically excited state. The energy of the excited valence electron in the In*-He_N system is a very sensitive probe for the temporal evolution of the He environment because of strong Pauli repulsion with the surrounding helium [23]. TRPES measures the transient PE kinetic energy, which additionally depends on a temporal shift of the ionic state energy ($E_{\text{HeN-In}^+}$, figure 4b). Therefore, we use TDDFT modeling of the photoexcitation process in order to distinguish these two contributions. Previously, TDDFT simulations could only be compared to time-dependent experiments at the weakly-interacting droplet surface [16]. In the interior, the dopant-He interaction is much stronger, with the consequence that significantly more excess energy ($270 \text{ meV} \approx 2200 \text{ cm}^{-1}$ in our case) is coupled into the system during photoexcitation, challenging the accuracy of the TDDFT approach. The reproduction of the observed transient PE peakshift by TDDFT (figures 2a and 4c), without using any experimental input for the simulation, demonstrates that a simulation of photoexcitation dynamics is possible even in the case of significant excess energy.

By combining experiment and theory we obtain the following mechanistic picture of the coupled, ultrafast electronic and nuclear relaxation process: Photoexcitation increases the radial expansion of the valence electron wave function, as is suggested by the strong repulsive part of the In-He pair potential at short distances in the excited state (Supplementary Fig. 3). Pauli repulsion between the extended electron density and the closed-shell He thereby pushes the surrounding solvation shell away (see Supplementary Movie 1). The spherical He bubble containing the excited In atom almost doubles its radius from 4.5 Å to 8.0 Å within 600 fs after excitation (figures 1b and 4a). This process can also be explained with the corresponding potential energy surfaces (figure 1a): Because the equilibrium bubble radius of the excited electronic state is larger than that of the ground state, photoexcitation causes enlargement of the solvation shell. This nuclear relaxation can be followed as transient PE peak shift because the potential energies of the excited state and the ionic state depend on the distance of neighboring He atoms to the In dopant. From an energetic viewpoint, the bubble expansion is accompanied by the conversion of electronic energy into kinetic energy of the He atoms, as illustrated by the mirror-imaged progression of the two corresponding curves (excited state interaction energy $E_{\text{HeN-In}^*}$ and kinetic energy of the He atoms $E_{\text{kin, He}}$) in figure 4b. The minute decrease of the sum of $E_{\text{HeN-In}^*}$ and $E_{\text{kin, He}}$ over time represents energy transferred to He-He interactions (correlation energies).

The impulsive stimulation of the He solvation layer initiates a collective oscillation of the He bubble, the first contraction of which is observed as increase of the PE kinetic energy and linewidth in figure 3 at (28 ± 1) ps, induced by the temporally increased He density in the vicinity of the In atom. The repulsive character of the excited state In-He pair potential (see Supplementary Note 2 and Supplementary Fig. 3) leads to ejection of the In atom from the droplet on a time scale of about 60 ps (see Supplementary Movie 2). Consequently, the PE kinetic energy decreases to the free-atom value within this time span (see figure 3) and only one bubble oscillation can be observed. Dopant ejection is further confirmed by observing a rise in photoion yield on the same time scale (Supplementary Fig. 7a) and a transient change of the linewidth of the PE peak (see figure 3 and Supplementary Fig. 7b). While the TDDFT simulation assumes a fixed starting location of the In atom, the experimentally observed ensemble comprises a distribution of In atoms within the droplet. As a consequence, the timing of the first bubble contraction will appear smeared out in the experimental data, because the PE energy peak shift due to dopant ejection is superimposed on

the pure bubble oscillation. Photoexcitation of the In dopant in the centre of the droplet induces multiple oscillations and no ejection within the simulated time span (see Supplementary Movie 3 and Supplementary Note 4). We therefore conclude, that the collective solvation shell oscillation has a period of about 30 ps, the observation of which provides insight into the hydrodynamics of the bubble in real time [24].

In conclusion, our experiments prove that ultrafast, coupled electronic and nuclear dynamics of particles located inside superfluid He nanodroplets can be observed and simulated. The expansion of the dopant solvation shell will be superimposed on any molecular relaxation dynamics on femtosecond time scales inside the droplet. When applying photoelectron detection, which seems to be a promising observable for intrinsic molecular dynamics inside helium droplets, the photoelectron transients induced by solvation shell dynamics have to be known. The duration of dopant ejection, on the other hand, limits the time frame for which ultrafast reactions inside the quantum fluid can be observed. As a proof of concept, our results pave the way to use helium droplets as a novel sample preparation technique for ultrafast studies on previously inaccessible tailor-made or fragile molecular systems.

Methods

Helium droplet generation and In atom pickup

Helium droplets with an average size of about 4000 atoms are generated by supersonic expansion of high purity (99.9999 %) helium gas through a cooled nozzle (5 μm diameter, 18 K temperature, 40 bar stagnation pressure) into high vacuum. The expansion in combination with evaporative cooling results in droplet temperatures of about 0.4 K, which is well below the superfluid phase transition of helium. The He_N are doped with In atoms inside a pickup region, where indium is resistively heated. Pickup conditions are optimized for single atom pickup and for an acceptable signal-to-noise ratio. Indium was chosen as dopant because of its simple electronic structure with one valence electron and because its excited state is symmetric, simplifying the TDDFT simulations, as well as the interpretation. After passing a differential pumping stage to increase the vacuum quality, the doped droplets enter the measurement chamber, where the He_N beam is crossed at right angle by the femtosecond laser pulses inside the extraction region of a time-of-flight spectrometer.

Time-resolved photoelectron spectroscopy

A commercial Ti:sapphire femtosecond laser system (Coherent Vitara oscillator, Legend Elite Duo amplifier) delivers 25 fs laser pulses with 800 nm central wavelength and 4 mJ pulse energy at a repetition rate of 3 kHz. The pulses are split into a pump and a probe path with variable time delay. Pump pulses are frequency up-converted by an optical parametric amplifier (Coherent OPerA Solo) that tunes the wavelength to 376 nm (3.30 eV, 6 nm \approx 60 meV full width at half maximum, FWHM). Probe pulses are frequency doubled to 405 nm (3.06 eV) with a 1 mm thick BBO crystal (3 nm \approx 25 meV, FWHM) for short delays and with a 5 mm thick LBO crystal (1.5 nm \approx 10 meV, FWHM) for long delays and guided over a delay stage. Dichroic mirrors are used in both beam paths to remove undesired wavelengths from the upconversion process. Pump and probe pulses are focused into the extraction region of the linear time-of-flight spectrometer, where they overlap

in space and time at the intersection region with the He_N beam. A magnetic bottle configuration [25] ensures high electron detection efficiency and a small positive repeller voltage of a few hundred mV increases the electron kinetic energy resolution. At these parameters we estimate the relative energy resolution of the spectrometer to be about 10%, based on reference measurements. PE energies are calibrated with the free atom line, which position is retrieved by subtraction of the excited state binding energy [26] from the probe photon energy. The measurement chamber is operated at a base pressure of 10^{-10} mbar.

The intensities of the pump and probe pulses are optimized to obtain a maximum pump-probe signal with respect to pump-only and probe-only backgrounds. The pump wavelength for In excitation to the lowest excited state ($5s^26s$) is chosen to be 376 nm in order to optimize the monomer to dimer ratio (see Supplementary Note 1 and Supplementary Fig. 2), which is blue-shifted by 270 meV with respect to the gas-phase excitation wavelength at 410 nm [26]. This amount of excess energy is coupled into the In- He_N system at photoexcitation. The pump-probe cross correlation is estimated with 150 fs.

Time-dependent helium density functional theory

In the last years the approach of TDDFT for the bosonic system of helium has been successfully applied to describe the dynamical interaction of surface- and centre-located species with the helium quantum fluid, providing important insight into effects like superfluidity on the microscopic level [27], desorption dynamics [16], or collision processes [28, 29].

Details on the application and formalism of static and dynamic HeDFT are given elsewhere [22] and the computing package of the BCN-TLS group is available to the public as open source [21]. Here only the basic concepts and the terms that affect the presented results are given: Both static and dynamic computations are based on the Orsay-Trento functional [30], which attributes for He-He interactions, and the diatomic In-He potential energy surfaces. These pair potentials were calculated with high level ab initio methods for the ground, excited and ionic state (see Supplementary Note 2 and Supplementary Fig. 3). The simulations are performed for a He_{4000} droplet with the In impurity located in the centre by using a He-functional that includes the solid term [31]. We use a three dimensional Cartesian box of 96 Å length with a discrete grid size of 320 pt (0.3 Å spacing) and time steps of 0.1 fs to simulate the bubble expansion dynamics within the first ps and a grid size of 256 pt (0.375 Å spacing) and time steps of 1 fs for the bubble oscillation dynamics up to 100 ps. For the bubble oscillation dynamics the starting position was chosen to be at 20 Å distance to the centre, which leads to a similar ejection behavior as in the experiment. Both the bubble expansion and the oscillation period are local effects and are found to be very similar for dopant locations in the droplet centre. With the statically optimized ground state He density, a dynamical evolution is triggered by replacing the ground state pair potential with the excited state pair potential. This instantaneous perturbation drives the system and TDDFT allows to follow the resulting dynamics in real time [22], by solving the TDDFT equations for the helium and Newton's equations of motion for the impurity. Photoelectron spectra are simulated by integrating the pair potential energies $E_{\text{He-In}}$ over the whole droplet density ρ_{He} for both the excited and the ionic state for various timesteps in the simulation. The difference between the interaction energies directly compares to the difference in ionization energy of the immersed impurity and therefore to the shift in PE energy:

$$\text{PE shift (t)} = \int \rho_{\text{He}}(\mathbf{r}, t) E_{\text{In}^*-\text{He}}(\mathbf{r} - \mathbf{r}_{\text{In}^*}(t)) \, d\mathbf{r} - \int \rho_{\text{He}}(\mathbf{r}, t) E_{\text{In}^+-\text{He}}(\mathbf{r} - \mathbf{r}_{\text{In}^+}(t)) \, d\mathbf{r}$$

Since a huge amount of energy is deposited into the system in the excitation process, the simulations were tested for numerical uncertainties by variation of different parameters (grid size, time step and cutoff energy), as presented in Supplementary Note 3 and Supplementary Figs. 4-5.

Data availability

The data measured, simulated and analysed in this study are available from the corresponding author on reasonable request.

References

- [1] Zewail, A., De Schryver, F., De Feyter, S. & Schweitzer, G. *Femtochemistry: With the Nobel Lecture of A. Zewail* (Wiley, 2001).
- [2] Townsend, D. *et al.* The roaming atom: straying from the reaction path in formaldehyde decomposition. *Science* **306**, 1158–1161 (2004).
- [3] Blanchet, V., Zgierski, M. Z., Seideman, T. & Stolow, A. Discerning vibronic molecular dynamics using time-resolved photoelectron spectroscopy. *Nature* **401**, 52–54 (1999).
- [4] Calegari, F. *et al.* Ultrafast electron dynamics in phenylalanine initiated by attosecond pulses. *Science* **346**, 336–339 (2014).
- [5] Callegari, C. & Ernst, W. E. Helium droplets as nanocryostats for molecular spectroscopy - from the vacuum ultraviolet to the microwave regime. In Merkt, F. & Quack, M. (eds.) *Handbook of High Resolution Spectroscopy* (John Wiley & Sons, Chichester, 2011).
- [6] Toennies, J. P. & Vilesov, A. F. Superfluid helium droplets: A uniquely cold nanomatrix for molecules and molecular complexes. *Angew. Chem. Int. Ed.* **43**, 2622–2648 (2004).
- [7] Koch, M., Auböck, G., Callegari, C. & Ernst, W. E. Coherent spin manipulation and ESR on superfluid helium nanodroplets. *Phys. Rev. Lett.* **103**, 035302 (2009).
- [8] Shepperson, B. *et al.* Laser-induced rotation of iodine molecules in helium nanodroplets: revivals and breaking free. *Phys. Rev. Lett.* **118**, 203203 (2017).
- [9] Chatterley, A. S., Shepperson, B. & Stapelfeldt, H. Three-dimensional molecular alignment inside helium nanodroplets. *Phys. Rev. Lett.* **119**, 073202 (2017).
- [10] Nauta, K. & Miller, R. E. Formation of cyclic water hexamer in liquid helium: the smallest piece of ice. *Science* **287**, 293–295 (2000).
- [11] Nauta, K. & Miller, R. E. Nonequilibrium self-assembly of long chains of polar molecules in superfluid helium. *Science* **283**, 1895–1897 (1999).
- [12] Higgins, J. *et al.* Photoinduced chemical dynamics of high-spin alkali trimers. *Science* **273**, 629–631 (1996).
- [13] Gutberlet, A. *et al.* Aggregation-induced dissociation of $\text{HCl}(\text{H}_2\text{O})_4$ below 1 K: the smallest droplet of acid. *Science* **324**, 1545–1548 (2009).

- [14] Ziemkiewicz, M. P., Neumark, D. M. & Gessner, O. Ultrafast electronic dynamics in helium nanodroplets. *Int. Rev. Phys. Chem.* **34**, 239–267 (2015).
- [15] Mudrich, M. & Stienkemeier, F. Photoionisation of pure and doped helium nanodroplets. *Int. Rev. Phys. Chem.* **33**, 301–339 (2014).
- [16] von Vangerow, J. *et al.* Imaging excited-state dynamics of doped He nanodroplets in real-time. *J. Phys. Chem. Lett.* **8**, 307–312 (2017).
- [17] Loginov, E., Rossi, D. & Drabbels, M. Photoelectron spectroscopy of doped helium nanodroplets. *Phys. Rev. Lett.* **95**, 163401 (2005).
- [18] Hertel, I. V. & Radloff, W. Ultrafast dynamics in isolated molecules and molecular clusters. *Rep. Prog. Phys.* **69**, 1897–2003 (2006).
- [19] Stolow, A., Bragg, A. E. & Neumark, D. M. Femtosecond time-resolved photoelectron spectroscopy. *Chem. Rev.* **104**, 1719–1757 (2004).
- [20] Wang, C. C. *et al.* Photoelectron imaging of helium droplets doped with Xe and Kr atoms. *J. Phys. Chem. A* **112**, 9356–9365 (2008).
- [21] Pi, M. *et al.* ⁴He-DFT BCN-TLS: a computer package for simulating structural properties and dynamics of doped liquid helium-4 systems. <https://github.com/bcntls2016/> (2016).
- [22] Ancilotto, F. *et al.* Density functional theory of doped superfluid liquid helium and nanodroplets. *Int. Rev. Phys. Chem.* **36**, 621–707 (2017).
- [23] von Haeften, K., Laarmann, T., Wabnitz, H. & Möller, T. Bubble formation and decay in ³He and ⁴He clusters. *Phys. Rev. Lett.* **88**, 233401 (2002).
- [24] Moroshkin, P., Hofer, A. & Weis, A. Atomic and molecular defects in solid ⁴He. *Phys. Rep.* **469**, 1–57 (2008).
- [25] Kruit, P. & Read, F. H. Magnetic field paralleliser for 2 π electron-spectrometer and electron-image magnifier. *J. Phys. E: Sci. Instrum.* **16**, 313–324 (1983).
- [26] Kramida, A., Yu. Ralchenko, Reader, J. & and NIST ASD Team. NIST Atomic Spectra Database (version 5.5.2), [Online]. Available: <https://physics.nist.gov/asd> [Fri Jan 19 2018]. National Institute of Standards and Technology, Gaithersburg, MD (2018).
- [27] Brauer, N. B. *et al.* Critical Landau velocity in helium nanodroplets. *Phys. Rev. Lett.* **111**, 153002 (2013).
- [28] Leal, A., Mateo, D., Hernando, A., Pi, M. & Barranco, M. Capture of heliophobic atoms by ⁴He nanodroplets: the case of cesium. *Phys. Chem. Chem. Phys.* **16**, 23206–23213 (2014).
- [29] Coppens, F., Ancilotto, F., Barranco, M., Halberstadt, N. & Pi, M. Capture of Xe and Ar atoms by quantized vortices in ⁴He nanodroplets. *Phys. Chem. Chem. Phys.* **19**, 24805–24818 (2017).
- [30] Dalfovo, F., Lastri, A., Pricauptenko, L., Stringari, S. & Treiner, J. Structural and dynamical properties of superfluid helium: a density-functional approach. *Phys. Rev. B* **52**, 1193–1209 (1995).
- [31] Ancilotto, F., Barranco, M., Caupin, F., Mayol, R. & Pi, M. Freezing of ⁴He and its liquid-solid interface from density functional theory. *Phys. Rev. B* **72**, 214522 (2005).

Acknowledgements

We thank Manuel Barranco, Martí Pi and the whole BCN-TLS-HeDFT-code team for their support with technical details of the simulations and fruitful discussions. We appreciate the experimental support by Miriam Meyer and acknowledge financial support by the Austrian Science Fund (FWF) under Grant P29369-N36, as well as support from NAWI Graz.

Supplementary information for

Femtosecond photoexcitation dynamics inside a quantum
solvent

Thaler et al.

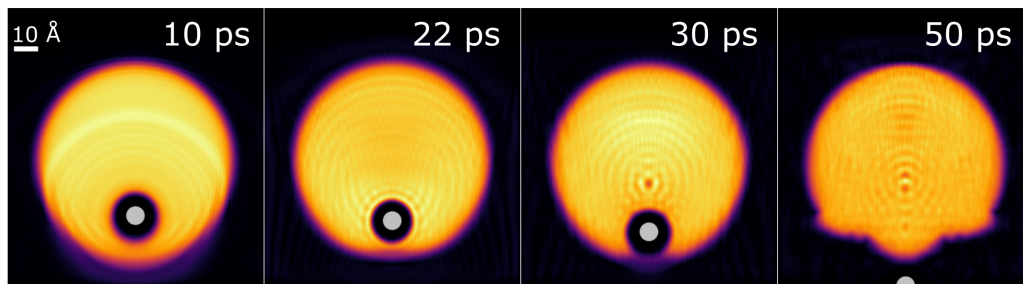


Figure 5: Snapshots from Supplementary Movie 2. Helium density distributions of a He_{4000} droplet with an indium atom, originally located at 20 \AA distance to the center, as obtained with TDDFT for characteristic time delays. The dopant is ejected from the droplet after 60 ps , accompanied by a contraction of the solvation shell (bubble) around 22 ps .

Supplementary Note 1: The In- He_N excitation spectrum

The In- He_N excitation spectrum in the region of the In $5s^26s \leftarrow 5s^25p$ transition was previously recorded and is shown in Supplementary Fig. 6. In addition to the monomer signal (blue line) an In dimer band (red line) appears with strong overlap to the monomer. The monomer signal shows a maximum at 368 nm , which is blue-shifted by 2800 cm^{-1} with respect to the free atom line (green, solid line) [1]. The excitation wavelength was chosen at 376 nm (black, dashed line) to obtain a good monomer-to-dimer ratio. Additionally, a reduced pickup temperature was used to minimize the dimer influence.

Supplementary Note 2: The In-He pair potentials

The most important inputs for both the static and time-dependent DFT simulations are the dopant-helium diatomic potential energy surfaces for all electronic states that are populated in the experiment. The spin-orbit coupling corrected energy curve of the ground state ($X^2\Pi_{1/2}$), the first excited state ($2^2\Sigma_{1/2}$) and the ionic state of the In-He molecule are shown in Supplementary Fig. 7. All three states are spherically symmetric and the spin-orbit splitting of the ground state to the $^2P_{3/2}$ ($1^2\Pi_{3/2}$ and $1^2\Sigma_{1/2}$, not shown in Supplementary Fig. 7) has a value of about 2000 cm^{-1} , for which reason the latter is not taken into account in the simulation.

For completeness, we give a short summary of the ab initio strategy: In the calculation, the aug-cc-pV5Z family of basis sets [2, 3] in combination with the ECP28MDF effective core potential of the Stuttgart/Köln group [4] is used. The ab initio calculations are performed with the MOLPRO software package [5]. To account for the weak van der Waals-type binding between the He and In, a combination of multiconfigurational self consistent field calculations (MCSCF) [6, 7] and multireference configuration interaction (MRCI) [8, 9] is applied. The active space of the MRCI approach consists of three valence electrons, the core orbitals are optimized in the MCSCF calculation and kept doubly occupied. The curves are basis set-extrapolated by applying additional calculations with the aug-cc-pVQZ and aug-cc-pVTZ basis set families and the three-point extrapolation formula by Wilson and Dunning [10]. By using the Breit-Pauli operator, the spin-orbit splitting is calculated.

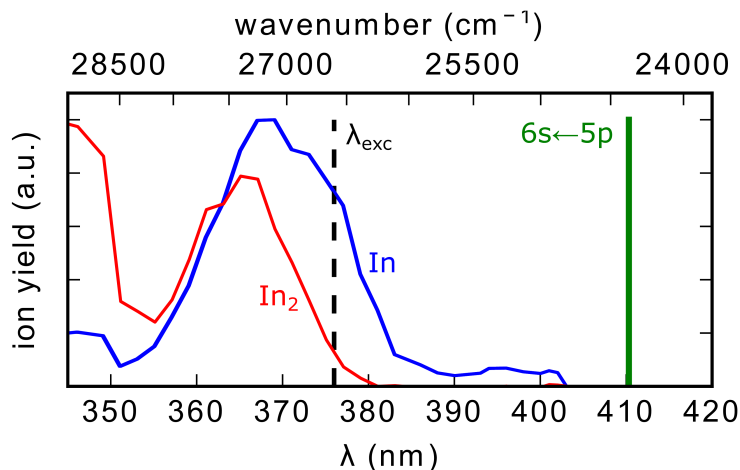


Figure 6: Excitation spectrum of the indium monomer (In) and the indium dimer (In_2), both solvated inside He_N . The spectra are measured in a pump-probe experiment with 200 ps time delay and photoion detection at the In monomer mass (115 amu) and the In dimer mass (230 amu), respectively. The pump-probe delay time is sufficiently long that both monomers and dimers are ejected from the droplet and ionized in the gas phase. The spectra were recorded at a higher In pickup temperature as the presented experiments in order to obtain a stronger dimer signal. Additionally, the gas phase In transition (green, solid line) and the applied excitation wavelength (black, dashed line) are indicated.

Supplementary Note 3: Numerical error tests for the simulation

The large amount of 270 meV excess energy coupled to the system in the photoexcitation process, which is represented as high blueshift of the in-droplet excitation wavelength with respect to the free atom line (see Supplementary Fig. 6), is connected to an equally high amount of excited state interaction energy $E_{\text{He}_N\text{-In}^*}$ (Fig. 3b in the main manuscript). This situation requires a careful choice of the simulation parameters in order to avoid numerical errors. For example, the He repulsion by the excited state electronic wave function of the In atom causes a strong increase in the kinetic energy of the He. A correct description of the He movement requires a fine grid size and small time steps, especially within the first few fs, where the acceleration is high. We test for numerical errors by calculating the transient change of $E_{\text{He}_N\text{-In}^*}$ for different grid sizes and different time steps, as shown in Supplementary Figs. 8 and 9.

The grid sizes used for the simulations presented in the paper are 320 pt for simulation of the bubble expansion dynamics (0 to 1 ps) and 256 pt to simulate the bubble oscillation (0 to 100 ps). Supplementary Fig. 8c shows that for the short dynamics an increase to 384 pt does not change the interaction energy significantly, while a decrease to 256 pt would introduce errors on the order of about 1%. A similar behavior is observed for the higher timescales (see Supplementary Fig. 8d), where a grid size of 192 pt introduces numerical errors that are on the order of the simulated energies, whereas nearly no deviation to the grid size of 320 pt is found.

The influence of the time step parameter turned out to be less pronounced, as shown in Supplementary Fig. 9c. An increase from 0.10 fs, as used for the shorter bubble expansion simulations,

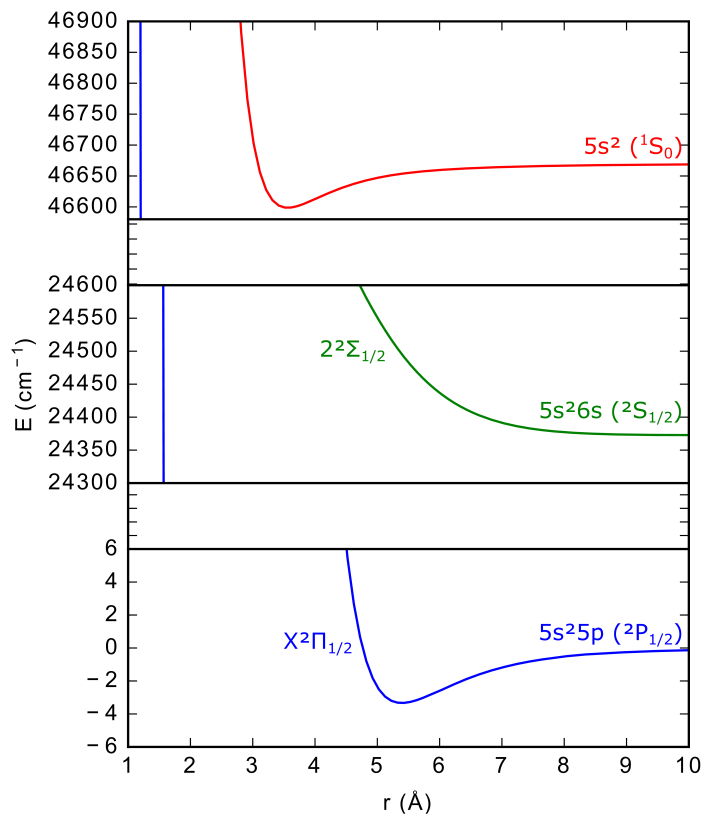


Figure 7: Indium-Helium interaction pair potentials used for the DFT and TDDFT simulations. Ground state (blue), first excited state (green) and ionic state (red).

to 0.50 fs gives a slightly stronger change of $E_{\text{HeN-In}^*}$, as compared to a decrease to 0.05 fs, both of which are, however, in the 10^{-10} eV range. The influence on the simulation for the longer bubble oscillation (simulated with 1 fs steps) is an order of magnitude higher (see Supplementary Fig. 9d), but still remains in the 10^{-9} eV range.

Another important parameter is the cutoff-energy for the different pair potentials, that has to be chosen high enough in order to avoid unphysical He density cumulations and energetic instabilities. The cutoff-energies for the ground state, the excited state and the ionic state potential are chosen with 2150 cm^{-1} , 1008 cm^{-1} and 5560 cm^{-1} , respectively. As the excited state cutoff-energy has the lowest value, different energies around 1008 cm^{-1} were tested with the result that the influence on the excited state interaction energy was below 10^{-10} eV (not shown).

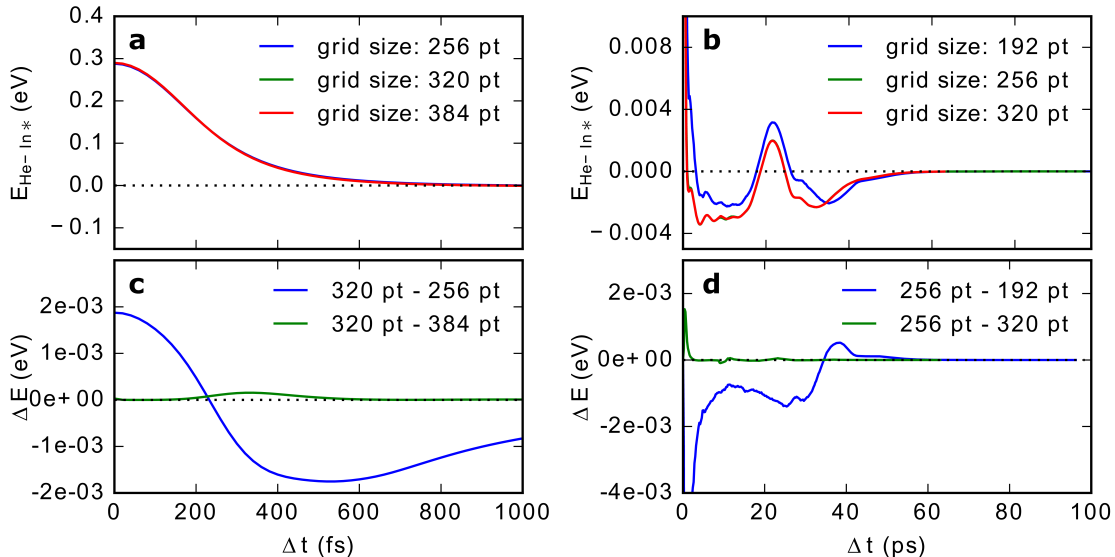


Figure 8: Dependence of the excited state interaction energy $E_{\text{He-In}^*}$ on the grid size parameters. (a) $E_{\text{HeN-In}^*}$ as function of time within the first picosecond for three different grid sizes of 256, 320 and 384 pts, calculated with 0.10 fs time steps. (b) $E_{\text{HeN-In}^*}$ for higher time delays for grid sizes of 192, 256 and 320 pt, calculated with 1 fs time steps. (c) Difference of interaction energy obtained with 320 pt grid size to that obtained with 256 and 384 pt, respectively. (d) Difference of interaction energy obtained with 256 pt grid size to that obtained with 192 and 320 pt, respectively.

Supplementary Note 4: Bubble dynamics for different locations inside the droplet

Whereas the simulated bubble expansion dynamics at short time delays (<1 ps) show no dependence on the position within the droplet where the dopant is photoexcited, the ejection process and the accompanied bubble oscillation observed at longer time delays are strongly dependent on the photoexcitation position. In Supplementary Fig. 10a the bubble radius over time for a starting location in the center of the droplet is shown, revealing a continued oscillation of the solvation shell with a period of about 30 ps and no ejection. This is in contrast to the 20 Å off-center excitation position, which shows only one contraction, superimposed to an overall increase of the radius due to the ejection. Supplementary Fig. 10b shows calculated PE peak energies as function of delay time for photoexcitation at various distances to the droplet center. The counter-propagating trends of bubble radius and PE energy for both the center and the 20 Å position clearly show that a contracted bubble coincides with an increased PE energy, which is a consequence of the increased In-He interaction energy of smaller bubbles (see Fig. 1 in the main manuscript). Different appearance times of the first contraction for different starting locations can be explained with the superimposed PE energy decrease due to ejection, as well as effects caused by helium shock-waves that propagate through the droplet following the initial bubble expansion (see Supplementary Movies 2 and 3).

We choose the simulation of the 20 Å starting position for comparison with the measured transient PE peak shift (Fig. 3 of the main text) because for other locations either multiple or no bubble

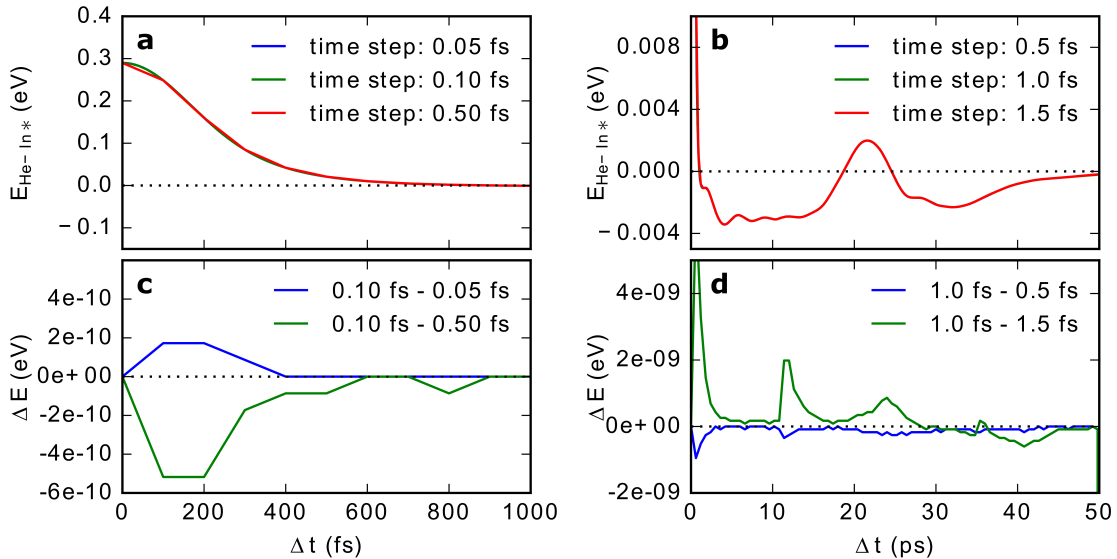


Figure 9: Dependence of the excited state interaction energy $E_{\text{He-In}^*}$ on the time step parameter. (a) $E_{\text{He-In}^*}$ within the first picosecond as function of time for three different time steps of 0.50, 0.10 and 0.05 fs, calculated with a grid size of 320 pt. (b) $E_{\text{He-In}^*}$ for higher timedelays for the time steps of 1.5, 1.0 and 0.5 fs, calculated with a grid size of 256 pt. (c) Difference of interaction energy obtained with 0.10 fs to that obtained with 0.50 fs and 0.05 fs, respectively. (d) Difference of interaction energy obtained with 1.0 fs to that obtained with 1.5 fs and 0.5 fs, respectively.

oscillations are predicted.

Supplementary Note 5: Transient ion yield and PE spectra at long time-delays

Ejection of the indium atoms can further be confirmed by a transient rise of ion yield. Because the ionic In^+ -He potential is strongly attractive, the atoms deeply solvate into the droplets when being ionized within or even in the vicinity of the droplets, in which case they are not detected. Only when escaped from the long-range, attractive potential of the droplet they are truly free and are measured [11]. This is seen in the transient ion yield (Supplementary Fig. 11a), where there is absent signal for the first 40 ps, followed by a signal rise within about 30 ps (to 67% of the maximum). The steady rise is connected to a position (and velocity) distribution of dopants inside the droplets before photoexcitation, resulting in an ensemble that gets ejected, which blurs the ion and electron transients. The same timescale of PE peak shift (Fig. 3 in main manuscript) and photoion yield rise confirms the correct interpretation of dopant ejection.

Further insight into the ejection process can be obtained from the line shapes of the PE lines. Supplementary Fig. 11b shows PE spectra obtained from In-He_N at time delays of 0.8 ps (blue line) and 200 ps (red line), as well as for bare In atoms (yellow line). Ionization inside the droplet at 0.8 ps leads to a shift of the PE peak to higher energies with respect to the bare atom due to the reduced ionization potential inside the droplet [12]. The PE spectrum is significantly broader

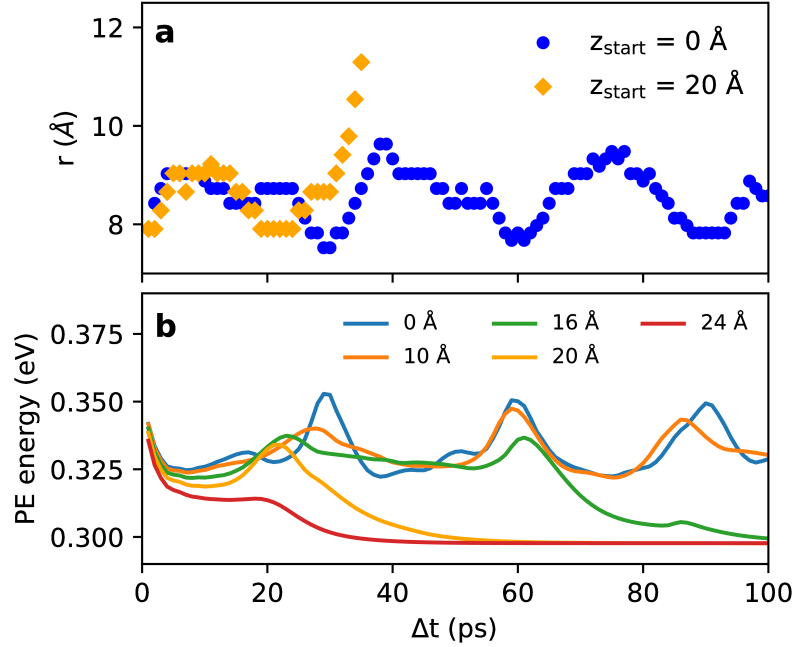


Figure 10: Comparison of the simulated In-He_N dynamics for photoexcitation at different positions. The bubble radius as function of time is shown in (a) and the corresponding transient change in photoelectron energy is shown in (b).

[(62 ± 2) meV, FWHM] compared to that of the bare atom [(35 ± 1) meV, FWHM] (see also Fig. 3 of the main text), which we ascribe to the Franck–Condon overlap of the excited and ionic potential energy surface inside the droplet. Additionally, the 0.8 ps spectrum shows a wing extending below the bare atom line, representing decelerated electrons [12], as discussed in the results section of the main text. Ionization of the In-He_N system at 200 ps gives exactly the same line shape as the bare atoms, proving that all In atoms are ejected from the droplets.

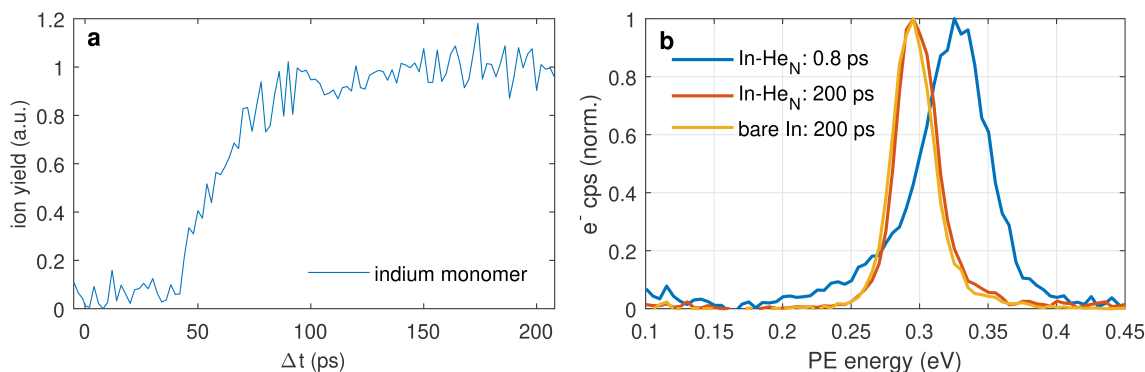


Figure 11: Transient photoion yield (a) and comparison of PE spectra at short and long time delays, as well as a PE spectrum of bare In atoms (b). The bare atom spectrum was recorded by deactivating the droplet source and exploiting the effusive In atom beam from the pickup source. The excitation wavelength for the bare indium spectrum was chosen with 410 nm (see Supplementary Fig. 6).

References

- [1] Kramida, A., Yu. Ralchenko, Reader, J. & and NIST ASD Team. NIST Atomic Spectra Database (version 5.5.2), [Online]. Available: <https://physics.nist.gov/asd> [Fri Jan 19 2018]. National Institute of Standards and Technology, Gaithersburg, MD (2018).
- [2] Woon, D. E. & Dunning-Jr., T. H. Gaussian basis sets for use in correlated molecular calculations. iv. calculation of static electrical response properties. *J. Chem. Phys.* **100**, 2975–2988 (1994). <https://doi.org/10.1063/1.466439>.
- [3] Peterson, K. A., Figgien, D., Goll, E., Stoll, H. & Dolg, M. Systematically convergent basis sets with relativistic pseudopotentials. ii. small-core pseudopotentials and correlation consistent basis sets for the post-d group 16–18 elements. *J. Chem. Phys.* **119**, 11113–11123 (2003). <https://doi.org/10.1063/1.1622924>.
- [4] Metz, B., Stoll, H. & Dolg, M. Small-core multiconfiguration-dirac-hartree-fock-adjusted pseudopotentials for post-d main group elements: Application to Pbh and Pbo. *J. Chem. Phys.* **113**, 2563–2569 (2000).
- [5] Werner, H.-J. *et al.* Molpro, version 2012.1, a package of ab initio programs (2012). See <http://www.molpro.net>.
- [6] Knowles, P. J. & Werner, H.-J. An efficient second order MCSCF method for long configuration expansions. *Chem. Phys. Lett.* **115**, 259–267 (1985).
- [7] Werner, H.-J. & Knowles, P. J. An efficient internally contracted multiconfiguration reference CI method. *J. Chem. Phys.* **89**, 5803–5814 (1988).
- [8] Knowles, P. J. & Werner, H.-J. Internally contracted multiconfiguration reference configuration interaction calculations for excited states. *Theor. Chem. Acc.* **84**, 95–103 (1992).
- [9] Boys, S. F. & Bernardi, F. The calculation of small molecular interactions by the differences of separate total energies. some procedures with reduced errors. *Mol. Phys.* **19**, 553–566 (1970).

- [10] Wilson, A. K. & Thom H. Dunning, J. Benchmark calculations with correlated molecular wave functions. x. comparison with “exact” mp2 calculations on ne, hf, h₂o, and n₂. *J. Chem. Phys.* **106**, 8718–8726 (1997). <https://doi.org/10.1063/1.473932>.
- [11] von Vangerow, J. *et al.* Imaging excited-state dynamics of doped He nanodroplets in real-time. *J. Phys. Chem. Lett.* **8**, 307–312 (2017).
- [12] Loginov, E., Rossi, D. & Drabbels, M. Photoelectron spectroscopy of doped helium nanodroplets. *Phys. Rev. Lett.* **95**, 163401 (2005).